

# Computational Study of Site-Specific Correlations among Oxygen Reduction Intermediates on Pd<sub>3</sub>Y (111)

Masoud Aryanpour\*

*Advanced Materials Lab, Samsung Advanced Institute of Technology, 255 Main Street, Cambridge, MA-02142, USA*

**Abstract:** In recent years, Pd<sub>3</sub>Y (111) alloy system has emerged as one of promising catalyst materials for oxygen reduction chemistry. This system is used in this work as a model system to study the site-specific adsorption energies of 4 ORR intermediates, O, OH, H<sub>2</sub>O, and OOH. Trends in energetics are estimated to assess the presence of scaling correlations among the adsorbates. Two types of site mappings are introduced and applied in correlating the energy of an adsorbed oxygen atom on hollow sites to its equivalent adsorption energies on top sites. Both types demonstrate relevant correlations to the other 3 intermediates, one correlates with OOH, and the other with H<sub>2</sub>O and OH. Discrepancies in energetic trends are explained in light of calculated charge densities and their implying effect on the observed correlations. OH and H<sub>2</sub>O strongly interact with the second layer of slab and the ground state adsorption of O, while OOH adsorption does not coincide with the second layer charge and correlates instead with its average effect that is reflected in the average adsorption energy of atomic oxygen. The results indicate how the energetics of one type of surface site may be affected by the energetics on another type. The underlying approach of site-mappings is expected to find high application in screening of catalyst materials using computational chemistry.

**Keywords:** Catalysts, doping, Oxygen reduction reaction, Activity screening, Surface sites, Computational chemistry, Site mappings.

## 1. INTRODUCTION

In recent decades, the fields of materials and surface sciences have been undergoing massive advances and fascinating developments. Most improvements are attributed to core technologies used by researchers that are capable to design, synthesize, and characterize novel materials geared toward target applications [1, 2]. Several modern spectroscopy techniques; such as TEM, STM, XES, NMR, and EXAFS; are being routinely used to help more traditional characterization tools of XRD and AFM. These fruitful practices enable one to determine not only chemical composition and crystal structure of the bulk material, but also and more elegantly provide very fine details of crystallinity, atomic orderings, and electron valence and band gaps [3-6].

Focusing on surface science studies of catalytic reactions, analyzing the measured spectra and detecting reaction intermediates, however, cannot be easily done without using ab-initio computations [7]. Computations can also explore different reaction pathways more straightforwardly than experiments [8, 9]. A set of fully computational frameworks [10], called high-throughput methods, have already been devised, and been put to screen materials based on theoretical metrics [11, 12].

In particular, computational screening of catalyst materials has been benefitting from a set of simplifying assumptions to avoid extensive calculations of the whole chemical mechanism. The scaling relations between various intermediates were established such that the adsorption energies of C, N, O on various transition metal elements shown to correlate well with CH<sub>x</sub>, NH<sub>x</sub>, and OH respectively [13-15]. Using scaling relations, DFT calculations are used to obtain adsorption energies of a key intermediate, for example atomic oxygen, on any candidate catalyst surface and predict its activity toward for instance oxygen reduction reaction (ORR). We refer the interested reader to theoretical descriptions of d-band center, which justify the observed scaling relations on the surfaces of single transition metal elements [16], and elucidate the reason for this simplifying computational framework.

Screening of catalysts activity, however, is far from being fully under realm of computational predictions. Extending the above computational strategies to other systems is accompanied with challenges of a different nature, for example, when one is interested in not pure elements but in alloys of elements. First, the bulk atomic structure of an alloy cannot be trivially determined and applied to computations. The number of permutations to arrange more than one element in the supercell model of a crystal explodes with increasing the number of sites. Fortunately, the total number of atomic arrangements can be reduced to the minimalist set using crystallographic symmetries [17]. The most stable atomic arrangement should still be

\*Address correspondence to this author at the Advanced Energy Lab, Samsung Advanced Institute of Technology, 255 Main Street, Cambridge, MA-02142, USA; E-mail: masoud@stanfordalumni.org

determined through calculating the energetics of the unique set of arrangements. Another resort is to use the results of in-situ characterization of concentration profile in the alloy material [18]. Obviously, performing such comprehensive and demanding experiments is not feasible and out of question in any high-throughput and screening type of study.

Another challenge in the computational study of an alloy catalyst lies in the heterogeneity of the alloy surface sites. The literature contains theoretical works that confirm selectivity of alloy surface sites. For example, the reactivity of (Cu, Pd, Au)/Ag toward ethylene epoxidation [19] is clearly a site-dependent reaction pathway. When screening for reactivity, the general situation is that the adsorption energy of each adsorbate does not come out the same on all sites but varies on different sites. The question is which value to use in the screening: an average on all sites, or that of the most favorable site, or something else? This question has not been considered or answered explicitly in the literature.

The surface heterogeneity is expected naturally to illustrate deviations from an ideal scaling relationship even when only a few exceptions are reported so far [16]. Despite the above challenges, exhaustive computations are carried out on various alloys and mixtures using the equivalent assumptions made for single element systems. While trends of activity are usually discussed, emphasized, and reported thoroughly, the relevant computational details about atomic configurations and surface sites, on which those results are based, are largely underscored or described scientifically insufficiently in the supplementary information. In the current work, instead, it has been attempted to provide all the computational details along with explicit computational assumptions that are found to be crucial in repeating this same study and in reproducing similar results. Thus, the mission of this work is to provide in-depth critical supports for previous alloy screening works [11, 20] and hopefully useful information for future research.

Using DFT calculations, this paper aims to delve into the question of relevant surface site on an alloy catalyst by studying correlations in the site-specific adsorption energies [21] of 4 intermediates of ORR on Pd<sub>3</sub>Y (111). The presence or absence of scaling correlations between adsorbates O, OH, H<sub>2</sub>O, and OOH are examined in careful details. The adsorption energies are evaluated and reported for all surface sites and correlations shown to exist. The Pd<sub>3</sub>Y alloy

system was chosen because of being screened as an important catalyst material with promising activity for oxygen reduction [20]. For its platinum-free composition, superior ORR activity and stability, it has been also patented as an inexpensive catalyst in fuel cells [22]. Additionally computations show this material can serve as a stable core for a Pt skin and can induce an anti-segregation force [23, 24].

## 2. COMPUTATIONAL METHOD

Periodic DFT calculations were carried out using ab-initio atomic simulation package VASP [25-28]. Density Functional Theory was applied to optimize the geometries by minimizing the total energy of the slab system (Figure 1). The exchange-correlation energy and potential were represented by the revised [29] flavor of Generalized Gradient Approximation Perdew-Burke-Ernzerhof pseudopotentials (GGA-PBE) [30, 31], and the Kohn-Sham one-electron valence states were described through using a plane waves basis with kinetic energy that fall below cutoff energy 500.0 eV (36.75 Ry). The Brillouin zone was sampled with a 4×4×1 scheme in x-y-z directions respectively by the automatic Monkhorst-Pack grid-generating technique. Other computational parameters were set at their default values provided by software VASP itself.

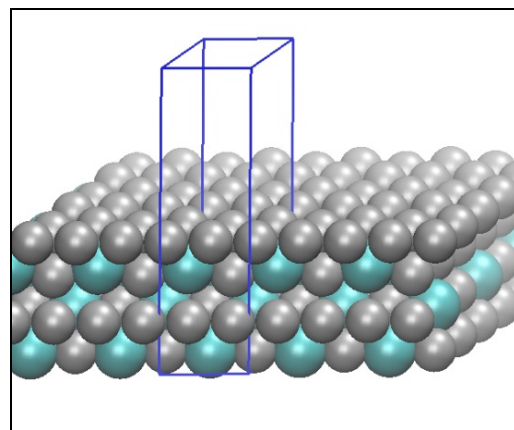


**Figure 1:** Bare slab model showing 12 Pd atoms and 4 Y atoms in the supercell.

The bare slab contains 16 transition metal atoms: 12 Pd and 4 Y, stacked in 4 closely packed layers each having 4 atoms. The concentration profile of Y atoms follows that of Ni in the experimentally determined structure of Pt<sub>3</sub>Ni [18]: no Y on the first/top layer counting from the adsorbate side, 2 on the second layer, and 1 on the rest two. The yttrium atoms were arranged in the supercell in such a way to maximize their configurational entropy in the structure. The

contribution of such entropy could play a dominant role in the total free energy of an alloy system [32].

In the structural optimization by DFT calculations, the top two layers of transition metals are allowed to relax in z-direction, while the lower two layers are fixed at their bulk locations. All atoms of adsorbates, on the other hand, are free to move in 3 coordinate directions. This combination in degrees of freedom provides the whole system with enough flexibility to represent close-to-real inter-atomic interactions in the system. Applying further degrees of freedom for the Pd and Y atoms, such as in-layer movements, is expected to have a secondary effect on the final results. The adsorbates and the topmost catalyst atoms are completely free to adjust their initial location and interact chemically also make or break their bonds in an ab-initio sense.

There exist 8 surface sites for the adsorption of an oxygen atom [33]: 4 fcc (F) and 4 hcp (H) as shown in Figure 2(a). The rest 3 adsorbates (OH, H<sub>2</sub>O, and OOH) are allowed to adsorb on 4 top (T) sites [34] as illustrated in Figure 2(b). It is known that for the adsorption of OH, bridge sites might also be favorable plus that the O<sub>2</sub> and H<sub>2</sub>O<sub>2</sub> species could form on the surface as well, leading to a probable H<sub>2</sub>O<sub>2</sub> dissociation mechanism [35]. Those are valid concerns and valuable topics for further research complementary to the current work, but not the main question for now.

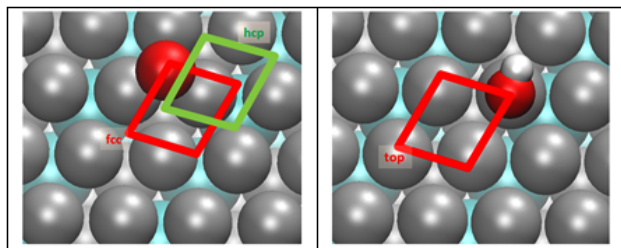


**Figure 2 (a):** Adsorption sites for O atom: 4 of type fcc, and 4 of type hcp **(b)** 4 top adsorption sites for OH, H<sub>2</sub>O, and OOH.

In Figure 3 the 12 sites have been labeled for easy referencing. The need for their explicit distinguishing and labeling becomes evident in the results discussions below, but the reason stems from the non-homogeneity of surface sites because of alloying Pd with Y. The numbering order of each 3 sets of F, H, and T sites in Figure 3 is not intended to reflect any prior steric or computational effect, nor any prior energetic preference.

In the supercell model used in this work, the differences in the activity/selectivity of the surface sites arise from not the first layer, which is composed of

equivalent Pd atoms only, but from the lower layers that are mixed/doped with Y atoms. No assumptions or filtering is employed for the activity of any site, and none is left out from the study. The unbiased treatment of surface sites is necessary to examine and to validate the scaling correlations. Considering the first and second layers only, one might be tempted to assume the equivalence of certain sites in Figures 2 and 3, for example sites T2 and T4, or H2 and H3. However, that tendency is not justified if the effect of the 3<sup>rd</sup> and 4<sup>th</sup> layers, seen from Figure 1, is taken into account too.

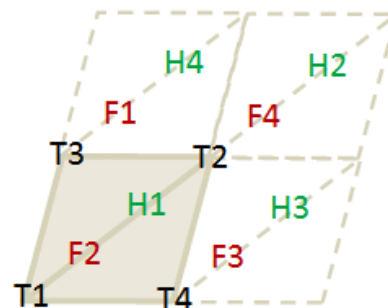


**Figure 3:** Labeling of surface sites: F1-F4 represent 4 fcc sites, H1-H4 are 4 hcp sites, and T1-T4 stand for 4 top sites.

The total number of calculated systems amounts to 21 = (8 = 2 × 4 sites for O) + (12 = 3 species on 4 sites) + (1 for bare slab Pd<sub>3</sub>Y (111)). Another 6 (1 for bare slab + 2 for O + 3 for the rest) on pure Pd (111) are computed to serve as the reference cases for reporting relative adsorption energies instead of the corresponding absolute values. Reason for utilizing Pd (111) as the reference system is to cancel out the contributions to the free energy because of Zero-Point-Energy (ZPE) and of entropy effects [36]. These contributions are associated with the adsorption of small molecules. Establishing discussions on only relative energetics hopefully removes most of the concern or worry whether a set of sufficiently accurate estimations of the above contributions were applied to adsorption energies or not. The remaining assumptions would be only the equality of ZPE and TΔS for each surface species on Pd (111) and Pd<sub>3</sub>Y (111). The relative adsorption energies would reflect selectively the effect of doping bulk Pd with yttrium.

### 3. RESULTS AND DISCUSSIONS

Atomic structures after optimization do not show any irregular drift of either slab atoms or adsorbate ions. The corresponding details are not of concern, and very unlikely to affect the discussions on activity or surface properties. The only noticeable effect is the upward movement of Y atoms on the second layer

**Table 1: Calculated Energies in Units of eV for Two Slab Systems Pd (111) and Pd3Y(111). Energies on the Latter System Depend on Sets of 4 Different Surface Sites 1-4, Arranged in 4 Columns. for example, Energy of O@hcp(1)=O@H1= -97.321088 eV**

slab	Pd(111)	Pd3Y (111)			
	-75.83862	-91.62311			
O@hcp (O@H)	-81.87413	-97.32109	-97.35347	-97.30204	-97.32169
O@fcc (O@F)	-82.06119	-96.78483	-96.96796	-97.47647	-97.47819
OH@top (OH@T)	-85.91211	-101.62702	-101.48950	-101.60145	-101.59985
H2O@top (H2O@T)	-90.63667	-106.40873	-106.36610	-106.40587	-106.36525
OOH@top (OOH@T)	-90.0918	-105.79285	-105.87119	-105.73534	-105.9299

toward the surface whenever an oxygen atom is adsorbed on an hcp site directly above. The upward motion of the Y atoms is an indication of segregation tendency in acidic environment [37, 23].

Table 1 reports the raw calculated energy values for 21 systems (for Pd3Y) + 6 (for Pd). For benchmarking purposes, let's examine oxygen adsorption on fcc that comes out by about 0.18 eV more favorable than on hcp site. This favorability is completely in agreement with previous works [38, 33]. Deciding between fcc and hcp is not as easy as one continues to the corresponding values on Pd3Y. There are 8 values instead of only two: 4 for fcc, and 4 hcp, whose order of stability for atomic oxygen would be: F4≈F3 > H2 > H1≈H4 > H3 > F1 > F2. The most favorable is still an fcc site, but also the most unfavorable one! Since coverage affects site occupations, the stability order reveals that at high O-coverage hcp sites could be occupied even more than fcc sites overall. The site-occupation behavior of atomic oxygen is by itself [39, 40], an interesting topic for which Monte-Carlo methods [41] would be useful, but out of this paper's scope.

The main question of interest is to seek the existence of scaling correlations among OH, H2O, OOH—that adsorb on top sites—and O—that adsorbs on hollow sites. For atop adsorbates, we define the top-site-specific relative adsorption energy as:

$$E_{ads}^{A@Ti} = (E_{Pd3Y}^{A@Ti} - E_{Pd3Y}^{slab}) - (E_{Pd}^{A@T} - E_{Pd}^{slab}), \quad (1)$$

Where  $T_i$  stands for any of 4 top sites in Figure 3,  $i$  is the site index  $i = \{1, 2, 3, 4\}$ , and  $A$  represents any on-top adsorbate  $A = \{OH, H_2O, OOH\}$ . Referencing energies with respect to pure Pd serves to two purposes. First it removes possible inaccuracies in estimation/calibration of ZPE and  $\Delta S$  of adsorbates if

their contributions would obscure the trends. Second, the referencing carves the effect of Y-doping out by subtracting and eliminating probable artifacts in DFT calculations.

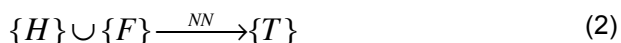
Corresponding energies can be plotted as functions of top sites T1-T4 easily. Representing energetics is not though as straightforward as in the case of O adsorption on hollow sites because there is no obvious way to represent the differing energetics. Should the minimum of 8 sites, that is most favorable case F4, be selected? A yes answer would have a difficult time justifying why there must be any correlation between one hollow site and energetics on all top sites. For instance, there is no reason why energetics of OH on T1 must be more related to F4, which is one farthest site to T1 in the cell, than the energetics of its immediate neighbors.

**Table 2: Neighborhood of 4 Top (T) Sites Each Surrounded by 3 hcp (H) and 3 fcc (F) Sites. See Figure 3 for Comparison. A Value of Unity Shows a Nearest Neighborhood (NN), While a Zero Stands for Lack of NN**

	H1	H2	H3	H4	F1	F2	F3	F4
T1	0	1	1	1	1	1	1	0
T2	1	0	1	1	1	0	1	1
T3	1	1	1	0	1	1	0	1
T4	1	1	0	1	0	1	1	1

Neighborhood of sites plays a significant role, and must be used as an influential factor in order to proceed with relating hollow sites to top sites. Nearest neighbors sites specific to each 4 top sites T1-T4 in Figure 3 are set up in Table 2: a value of unity shows a closest neighborhood, while a zero shows a lack of. The 6 NN of site T1 are H2-H4 plus F1-F3, not H1 nor

F4. The NN relationship then can be represented by a topological mapping:



where set  $\{\circ\}$  contains all sites of type  $\circ$  ordered by indices 1 to 4. The NN overlay represents the mapping matrix with the elements given by Table 2. Mapping relation [2] satisfies and reflects in an explicit way our chemical intuition that hollow sites nearest neighbors to any T site must have priority in affecting its energy than its farther hollow neighbors.

Further, to lump the energetics of 6 hollow sites that surround each T site (3 F + 3H in Figure 3) onto one value only, we need at least one 6-to-1 energy mapping scheme. Here two natural schemes are presented: 1) minimum energy of the 6 neighbor sites represented by  $\min(NN(.))$ , and 2) average of 6 energies of the neighbor sites, represented by  $\text{avg}(NN(.))$ :



The reason for defining the second scheme (4), in addition to the well-expected scheme (3), becomes clear subsequently.

Using energy mappings (3) and (4) from hollow sites to top sites, we can combine the adsorption energies of atomic O on the hcp and fcc sites for Pd3Y in Table 1, and find the equivalent energies on top sites. Plotting energy profile of 4 adsorbates O, OH, H2O, and OOH as function of T1-T4 becomes feasible, and would reveal the presence of correlations. A correlation must be present between two adsorbates if their energy curves follow similar trends on all sites, at least in a relative sense.

The results of relative adsorption energies indeed demonstrate correlations between energies of oxygen atom and those of OH, H2O, OOH; however not in the simplest possible way originally proposed in the literature [13], or at an expected level of energy tolerance (see below). There exists not just one single correlation but two correlational groups: the first group {OH, H2O} correlates with the first mapping  $\min(NN(hcp, fcc))$ , while group {OOH} matches the trends of  $\text{avg}(NN(hcp, fcc))$ .

Figures 4 and 5 illustrate the energetic trends of the above two groups. Accepting 38meV as the energy

threshold, the order of stability for OH, and O both follow  $T1 \approx T3 \approx T4 > T2$ . For H2O, the order differs slightly:  $T1 \approx T3 > T2 \approx T4$ . Those orders are in clear contrast to the site stability order in Figure 5:  $T2 \approx T4 > T1 \approx T3$  for both O and OOH; an opposite ordering compared to Figure 4.

These rather simple stability-ordering results render a few important points about the scaling relations for Pd3Y (111), and probably for many similar alloy systems. Firstly, non-oxygen ORR intermediates {OH, H2O, OOH}, adsorbed on top sites, can correlate quite differently with adsorbed atomic oxygen. It is seen that {OH, H2O} adsorption energies follow general trends of the ground state adsorption of O on the NN hollow sites. OOH on the other hand scales well with the average energetic of atomic oxygen on the 6 nearest neighbors fcc and hcp sites. To distinguish such differences, one must pay attention to what energy mapping is applied to Eq. (2).

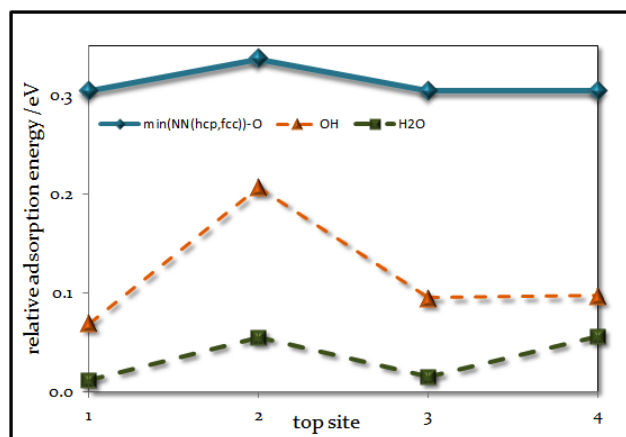


**Figure 4:** Adsorption energies of O using mapping relation (3), plus OH, and H2O on 4 top sites T1-T4 in Pd3Y(111) relative to Pd(111).

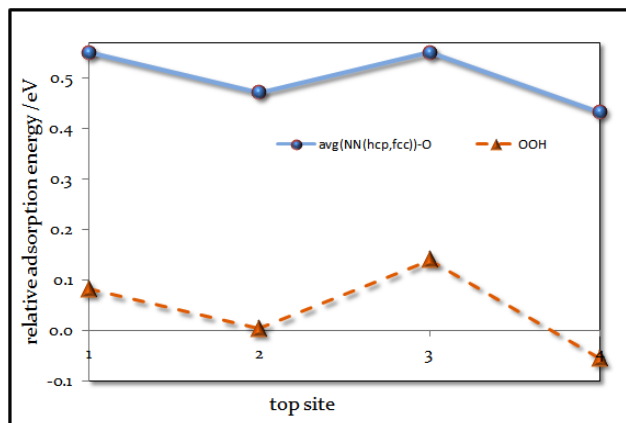


**Figure 5:** Adsorption energies of atomic O using mapping relation (4) is followed energetically by OOH on top sites T1-T4 in Pd3Y(111) relative to Pd(111).

Secondly, correlations among only the on-top adsorbates {OH, H<sub>2</sub>O, OOH} can face difficulties to be realized. The lack of sufficiently accurate scaling relations seems to be the sign of the need for using more than one site-mapping scheme. The absence of correlation in case OOH motivated defining another mapping scheme in relation (4). It should come also at no surprise if more complicated schemes would be necessary in more complicated alloys in order to seek and establish scaling relationships. Choosing a relevant mapping scheme might be useful to resolve current deviations from linear scaling that have been already shown to exist in some systems [16, 42].

Third, the choice of 38meV per adsorbate is not arbitrary, but is based on the ambient vibrational energy of molecules at room temperature ( $=3/2 k_B T$ ). An atomic configuration whose energy stands above this threshold with respect to the reference or the ground state system is considered less favorable. Two surface sites are considered equally favorable for an adsorbate if their corresponding energies fall within this energy threshold. Equivalency of two sites implies the feasibility that an adsorbate would feel in reaching another part of its adsorption energy landscape on a catalyst surface.

As temperature increases, so does the energy threshold, leading to accessibility of all sites to the adsorbate. Atomic oxygen therefore is expected to adsorb on both fcc and hcp sites at higher temperatures, although not with equal probabilities. As temperature rises, accessibility of all sites for all adsorbates does not progress at the same pace. A comparison of the curves in Figure 4 reveals that while the adsorption of O and H<sub>2</sub>O might occur on all sites at elevated temperatures, OH will continue to avoid site T2. For OH, this site is higher in energy by more than 100 meV compared to T1, T3, and T4. That is more than twice the relative instability of T2 for H<sub>2</sub>O,  $\approx 40$  meV.

Small differences in energy might be of little service in those cases where the prediction of main activity trends is all that is demanded. If screening of catalyst materials can tolerate the same energy fluctuations as the energy range on the adsorption sites, the sites selectivity problem would fade away, and simple scaling relationships might be working perfectly. However, different sites should be distinguished from each other if adsorption energies vary beyond a maximum tolerable value. In such a case, understanding reasons that lead to complicated sites

activity would be a valuable theoretical –computational tool of interest.

The validity of scaling relations among the ORR intermediates follows a similar course of relative importance. Depending on the level of required accuracy, the energetics of OOH in Figure 5 could be regarded as scaling with the energy curves of OH and H<sub>2</sub>O in Figure 4, or quite deviating from their trend. Theoretically, it would be important to rationalize the observed deviations that are disturbing a perfect matching in the adsorption behaviors. One such explanation is provided below based on the analysis of computed charge densities.

Remembering physical concepts behind density functional theory, energy must be a function of charge density in a very natural way. It is then expected that the electronic charge density of the surface of Pd<sub>3</sub>Y (111) interact with OOH rather distinctively than with OH, and H<sub>2</sub>O. Only the on-top adsorbates are being taken into account to start this discussion seeking only 1-to-1 site correspondence on T1-T4. Relation to hollow sites fcc and hcp is made subsequently through utilization of mapping relations (3) and (4).

Figures 6-8 depict the electronic charge around all on-top species mapped onto isosurfaces. The 2D plots are rotated in space to include the maximum density cross-section on the adsorbate for each case. These are the same planes that contain O—H bond and perpendicular to the slab surface.

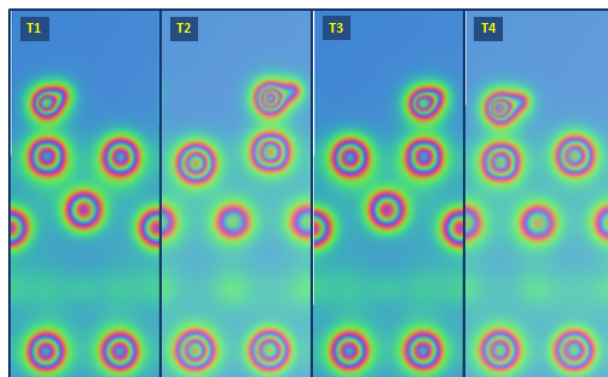


**Figure 6:** Charge density is surfaces of an adsorbed OH on Pd<sub>3</sub>Y(111). For each site T1-T4, the electronic charge of OH interacts strongly with charge at the second layer in the slab, but not with the charge on the third layer.

Small variations in charge are indeed seen comparing the interaction of the first slab layer with OH, H<sub>2</sub>O, and OOH. These could be safely disregarded in the current discussion in the favor of the second layer interaction. Both H<sub>2</sub>O and OH have maximized their

charge density on the O—H bond as with the maximum charge on the 2<sup>nd</sup> layer. This shows a strong electronic interaction with the transition metal atoms on the second layer in addition to the first. In a clear contrast, there is no such a positive interaction scenario between OOH and the second layer. The high concentration of charge on the OOH-containing plane matches the charge on this layer at a very low density, if not at its minimum.

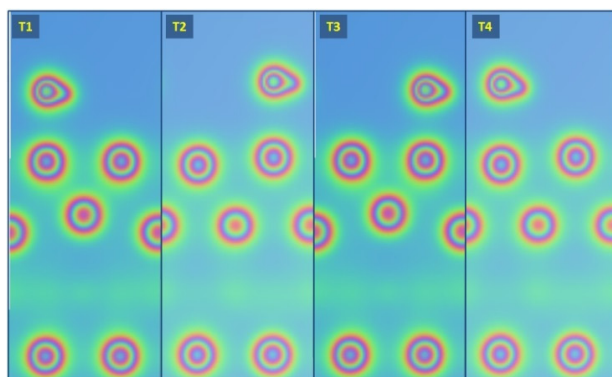


**Figure 7:** Charge density is surfaces of an adsorbed H<sub>2</sub>O on Pd<sub>3</sub>Y (111). For each site T1-T4, the electronic charge of H<sub>2</sub>O interacts strongly with charge at the second layer in the slab, but not with the charge on the third layer.

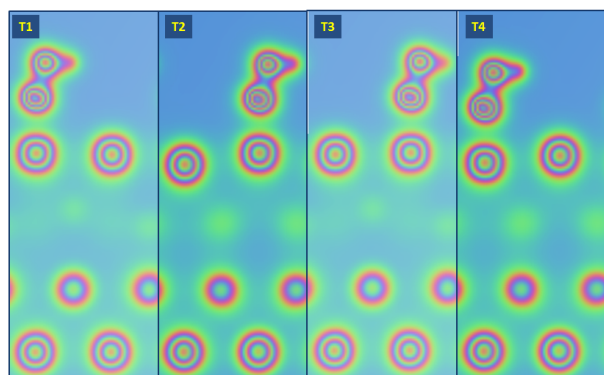


**Figure 8:** Charge density is surfaces of an adsorbed OOH on Pd<sub>3</sub>Y (111). At each site T1-T4, the electronic charge of OOH interacts only weakly, if at all, with charge at the second layer.

Going to the 3<sup>rd</sup> layer, the electron density takes on its minimum value for OH and H<sub>2</sub>O, while it adopts a much higher concentration for OOH (compare Figure 8 with 6 and 7). The reversal of site favorability for top sites, discussed above for Figures 4 and 5, could be attributed to this effect of reverse interaction behavior of charge density on the 2<sup>nd</sup> and the 3<sup>rd</sup> layers when bonded on with OOH. Whether or not this effect is caused inherently by alloying or in a more complicated way through the concentration profile of the alloy element –yttrium– will not change these variations. Rather, it redirects our attention back toward the

charge density as the underlying clue or cause of energy correlations or the lack of them.

The above analysis based on the charge density seems to be also capable of rationalizing two different mappings (3) and (4). Those mappings were suggested in order to seek correlations between the hollow sites as hosts of oxygen atom and top sites as hosts of OH, H<sub>2</sub>O, and OOH species. The first two adsorbates interact more strongly and positively with the second layer, causing their energetics to follow the trends of the minimum—or ground state—adsorption site of O among all neighboring hollow sites. The fcc and hcp hollow sites allow atom O to make a more impactful bond to the atoms on the second layer. The result of such a strong binding is reflected into the energy trends of O in Figure 4. The ground state site of atomic oxygen dominates the electronic charge around each one of the top sites through its strong bonding to the second layer of the slab.

The promoting effect of the second layer is largely lost in the case of OOH, whose energetic is affected instead by the average value of charge density of the second layer. That average charge density is represented by the adsorption energy (or concentration of charge) on all neighboring hollow sites. This average behavior is nothing than the mapping of hollow-to-top sites manifested by relation (4) and approved by Figure 5.

#### 4. CONCLUSION

This paper presented the results of DFT calculations on the adsorption of 4 ORR intermediates; O, OH, H<sub>2</sub>O, and OOH; on the (111) surface of Pd<sub>3</sub>Y. This alloy system has gained special attention because of its desired screened activity toward ORR chemistry. Massive screenings of pure and alloy systems are routinely performed relying on the validity of scaling relations between the ORR reaction intermediates.

It was shown that a perfect scaling is lacking between adsorption energies of OOH and those of OH or H<sub>2</sub>O. OOH energies do not follow the same site-specific fluctuations as OH and H<sub>2</sub>O do. The latter adsorbates show correlations with the ground state energy of the nearest neighbor oxygen atom. On the contrary, the former species agrees with the average adsorption energy of O on all nearest neighbors. The opposing energetic behavior of the intermediates was explained through the distinct interaction of the adsorbates with the slab second layer.

While charge distribution of an adsorbed OOH agrees quite weakly with the second layer of a slab model, OH and H<sub>2</sub>O interact with the same layer in a noticeably positive way. The result is OOH energetics varies much in line with the average of charge density on the slab second layer. In contrary, H<sub>2</sub>O and OH energies follow the trends of the ground state of atom O. Additionally, two types of hollow-to-top mappings were defined as simple analytical tools for relating the adsorption of O on the fcc and hcp sites to the top sites. It is expected that the presented combined analysis of energies, sites, and charge density would be able to explain site-specific adsorption behavior in other alloy systems. The site-mapping methodology, presented in this paper, could be employed in alloys or mixture of different catalyst materials when more accurate screening of activity is necessary.

## ACKNOWLEDGEMENTS

Parts of this work were done at Stanford University, and parts at Samsung AML.

## REFERENCES

- [1] Klabunde KJ, Richards R. *Nanoscale materials in chemistry*: Wiley Online Library; 2001.
- [2] Li Y, Somorjai GA. *Nanoscale advances in catalysis and energy applications*. *Nano letters*. 2010; 10(7): p. 2289-2295.
- [3] Scudiero L, Barlow DE, Mazur U, Hipps KW. Scanning tunneling microscopy, orbital-mediated tunneling spectroscopy, and ultraviolet photoelectron spectroscopy of metal (II) tetraphenylporphyrins deposited from vapor. *Journal of the American Chemical Society*. 2001; p. 4073-4080.
- [4] Bergmann UaPG. X-ray emission spectroscopy. *Photosynthesis research*. 2009; p. 255-266.
- [5] Bos AJ, Van Duijvenvoorde RM, Van der Kolk E, Drozdowski W, Dorenbos P. Thermoluminescence excitation spectroscopy: A versatile technique to study persistent luminescence phosphors. *Journal of Luminescence*. 2011; p. 1465-1471.
- [6] Cavallini A, Cavalcoli D, Polenta L. *Advanced Characterization Techniques*. In Pizzini S. *Advanced Silicon Materials for Photovoltaic Applications*. Chichester, UK: John Wiley & Sons, Ltd; 2012.
- [7] van Santen RA, aSP. *Computational methods in catalysis and materials science* Weinheim: Wiley-VCH; 2009.
- [8] Joshi AM. *Density Functional Theory (DFT) study of reaction pathways on gold and gold-alloy nanoclusters*: ProQuest; 2007.
- [9] Gajewski G, Pao CW. Ab initio calculations of the reaction pathways for methane decomposition over the Cu (111) surface. *The Journal of chemical physics*. 2011; p. 064707.
- [10] Christensen CH, Nørskov JK. A molecular view of heterogeneous catalysis. *The Journal of chemical physics*. 2008; 128(18): p. 182503.
- [11] Greeley J, Stephens IEL, Bondarenko A, Johansson TP, Hansen HA, Jaramillo TF, *et al.* Computational high-throughput screening of electrocatalytic materials for hydrogen evolution. *Nature materials*. 2006; 5(11): p. 909-913.
- [12] Curtarolo S, Hart GL, Nardelli MB, Mingo N, Sanvito S, Levy O. The high-throughput highway to computational materials design. *Nature materials*. 2013; 12(3): p. 191--201.
- [13] Abild-Pedersen F, Greeley J, Studt F, Rossmeisl J, Munter TR, Moses PG, *et al.* Scaling properties of adsorption energies for hydrogen-containing molecules on transition-metal surfaces. *Physical Review Letters*. 2007; 99(1): p. 016105.
- [14] Jones G, Bligaard T, Abild-Pedersen F, Nørskov JK. Using scaling relations to understand trends in the catalytic activity of transition metals. *Journal of Physics: Condensed Matter*. 2008; 20(6): p. 064239.
- [15] Andersson MP, Bligaard T, Kustov A, Larsen KE, Greeley J, Johannessen T, *et al.* Toward computational screening in heterogeneous catalysis: Pareto-optimal methanation catalysts. *Journal of Catalysis*. 2006; 239(2): p. 501-506.
- [16] Nørskov JK, Abild-Pedersen F, Studt F, Bligaard T. Density functional theory in surface chemistry and catalysis. *Proceedings of the National Academy of Sciences*. 2011; 108(3): p. 937-943.
- [17] Hart GLW, Nelson LJ, Forcade RW. Generating derivative structures at a fixed concentration. *Computational Materials Science*. 2012; p. 101-107.
- [18] Stamenkovic VR, Fowler B, Mun BS, Wang G, Ross PN, Lucas CA, *et al.* Improved oxygen reduction activity on Pt<sub>3</sub>Ni (111) via increased surface site availability. *Science*. 2007; 315(5811): p. 493-497.
- [19] Linic S, Jankowiak J, Barteau MA. Selectivity driven design of bimetallic ethylene epoxidation catalysts from first principles. *Journal of Catalysis*. 2004; 224(2): p. 489-493.
- [20] Greeley J, Stephens IEL, Bondarenko AS, Johansson TPHA, Jaramillo TF, Rossmeisl J, *et al.* Alloys of platinum and early transition metals as oxygen reduction electrocatalysts. *Nature chemistry*. 2009; 1(7): p. 552-556.
- [21] Matanovic I, Garzon FH, Henson NJ. Theoretical Study of Electrochemical Processes on Pt-Ni Alloys. *The Journal of Physical Chemistry C*. 2011; 115(21): p. 10640-10650.
- [22] Yoo SJ, Kim SK, Hwang SJ, Nam SW, Lim TH, Hong SA, inventors; Pd-Y alloy catalyst, method for preparing the same, and fuel cell comprising the catalyst. United States of America patent US 20110319256 A1. 2011 Dec 29.
- [23] Ramirez-Caballero GE, Ma Y, Callejas-Tovar R, Balbuena PB. Surface segregation and stability of core-shell alloy catalysts for oxygen reduction in acid medium. *Physical Chemistry Chemical Physics*. 2010; 12(9): p. 2209-2218.
- [24] Min HS, Choi SM, Seo JK, Noh SH, Kim WB, Han BC. The graphene-supported palladium and palladium-yttrium nanoparticles for the oxygen reduction and ethanol oxidation reactions: Experimental measurement and computational validation. *Applied Catalysis B: Environmental*. 2013; p. 163-171.
- [25] Hafner J, Kresse G. Ab initio molecular dynamics for liquid metals. *Physical Review B*. 1993; p. 558.
- [26] Hafner J, G. K. Ab initio molecular-dynamics simulation of the liquid-metal-amorphous-semiconductor transition in germanium. *Physical Review B*. 1994; p. 14251.
- [27] Kresse G, Furthmüller J. Efficient iterative schemes for ab initio total-energy calculations using a plane-wave basis set. *Physical Review B*. 1996; p. 11169.
- [28] Kresse G, Furthmüller J. Efficiency of ab-initio total energy calculations for metals and semiconductors using a plane-wave basis set. *Computational Materials Science*. 1996; p. 15.
- [29] Hammer B, Hansen LB, Nørskov JK. Improved adsorption energetics within density-functional theory using revised Perdew-Burke-Ernzerhof functionals. *Physical Review B*. 1999; p. 7413.

- [30] Perdew JP, Burke K, Ernzerhof M. Generalized gradient approximation made simple. *Physical Review Letters*. 1996; p. 3865.
- [31] Perdew JP, Burke K, Ernzerhof M. Erratum: Generalized gradient approximation made simple. *Physical Review Letters*. 1997; p. 1396.
- [32] Otto F, Yang Y, Bei H, George EP. Relative effects of enthalpy and entropy on the phase stability of equiatomic high-entropy alloys. *Acta Materialia*. 2013; p. 2628-2638.
- [33] Todorova M, Reuter K, Scheffler M. Oxygen Overlayers on Pd(111) Studied by Density Functional Theory. *Journal of Physical Chemistry B*. 2004; p. 14477-14483.
- [34] Roques J, Anderson AB, Murthi VS, Mukerjee S. Potential shift for OH (ads) formation on the Pt skin on Pt<sub>3</sub>Co(111) electrodes in acid theory and experiment. *Journal of the Electrochemical Society*. 2005; p. E193-E199.
- [35] Kattel S, Duan Z, Wang G. Density Functional Theory Study of an Oxygen Reduction Reaction on a Pt<sub>3</sub>Ti Alloy Electrocatalyst. *The Journal of Physical Chemistry C*. 2013; p. 7107-7113.
- [36] Rossmeis J, Logadottir A, Nørskov JK. Electrolysis of water on (oxidized) metal surfaces. *Chemical Physics*. 2005; p. 178-184.
- [37] Greeley J, Nørskov JK. Electrochemical dissolution of surface alloys in acids: Thermodynamic trends from first-principles calculations. *Electrochimica Acta*. 2007; p. 5829-5836.
- [38] Ganduglia-Pirovano M, Karsten Reuter V, Scheffler M. Stability of subsurface oxygen at Rh (111). *Physical Review B*. 2002; p. 245426.
- [39] Todorova M, Reuter K, Scheffler M. Density-functional theory study of the initial oxygen incorporation in Pd (111). *Physical Review B*. 2005; p. 195403.
- [40] Kitchin JR. Correlations in coverage-dependent atomic adsorption energies on Pd(111). *Physical Reviews B*. 2009; p. 205412.
- [41] Rai V, Aryanpour M, Pitsch H. First-principles analysis of oxygen-containing adsorbates formed from the electrochemical discharge of water on Pt (111). *The Journal of Physical Chemistry C*. 2008; p. 9760-9768.
- [42] Nørskov JK, Bligaard T, Rossmeis J, Christensen CH. Towards the computational design of solid catalysts. *Nature chemistry*. 2009; 1(1): p. 37-46

Received on 16-07-2014

Accepted on 19-08-2014

Published on 24-11-2014

<http://dx.doi.org/10.15379/2408-9834.2014.01.02.1>

© 2014 Masoud Aryanpour; Licensee Cosmos Scholars Publishing House.

This is an open access article licensed under the terms of the Creative Commons Attribution Non-Commercial License (<http://creativecommons.org/licenses/by-nc/3.0/>), which permits unrestricted, non-commercial use, distribution and reproduction in any medium, provided the work is properly cited.